






RESEARCH ARTICLE | SEPTEMBER 06 2023

Challenges in dynamic heat source modeling in high-power laser beam welding

Marcel Bachmann ; Antoni Artinov ; Xiangmeng Meng ; Stephen Nugraha Putra ; Michael Rethmeier 

 Check for updates

Journal of Laser Applications 35, 042003 (2023)

<https://doi.org/10.2351/7.0001079>



View
Online



Export
Citation

CrossMark



Journal of
Laser Applications

[Learn More](#)



RAPID TIME
TO ACCEPTANCE



COMMUNITY
DRIVEN



EXPANSIVE
COVERAGE



PRESTIGIOUS
EDITORIAL BOARD



EXTENSIVE
MARKETING


Challenges in dynamic heat source modeling in high-power laser beam welding

Cite as: J. Laser Appl. 35, 042003 (2023); doi: 10.2351/7.0001079

Submitted: 16 June 2023 · Accepted: 21 August 2023 ·

Published Online: 6 September 2023



Marcel Bachmann,¹  Antoni Artinov,¹  Xiangmeng Meng,¹  Stephen Nugraha Putra,¹ 
and Michael Rethmeier^{1,2,3} 

AFFILIATIONS

¹Bundesanstalt für Materialforschung und -prüfung (BAM), Unter den Eichen 87, 12205 Berlin, Germany

²Institute of Machine Tools and Factory Management, Technical University Berlin, Pascalstraße 8-9, Berlin 10587, Germany

³Joining and Coating Technology, Fraunhofer Institute for Production Systems and Design Technology, Pascalstraße 8-9, 10587 Berlin, Germany

Note: Paper published as part of the special topic on Proceedings of the International Congress of Applications of Lasers & Electro-Optics 2023.

ABSTRACT

The amount of absorbed energy in the keyhole as well as its spatial and temporal distribution is essential to model the laser beam welding process. The recoil pressure, which develops because of the evaporation process induced by the absorbed laser energy at the keyhole wall, is a key determining factor for the macroscopic flow of the molten metal in the weld pool during high-power laser beam welding. Consequently, a realistic implementation of the effect of laser radiation on the weld metal is crucial to obtain reliable and accurate simulation results. In this paper, we discuss manifold different improvements on the laser-material interaction, namely, the ray tracing method, in the numerical simulation of the laser beam welding process. The first improvement relates to locating the exact reflection points in the ray tracing method using a so-called cosine condition in the determination algorithm for the intersection of reflected rays and the keyhole surface. A second correction refers to the numerical treatment of the Gaussian distribution of the laser beam, whose beam width is defined by a decay of the laser intensity by a factor of $1/e^2$, thus ignoring around 14% of the total laser beam energy. In the third step, the changes in the laser radiation distribution in the vertical direction were adapted by using different approximations for the converging and the diverging regions of the laser beam, thus mimicking the beam caustic. Finally, a virtual mesh refinement was adopted in the ray tracing routine. The obtained numerical results were validated with experimental measurements.

Key words: laser beam welding, laser energy distribution, ray tracing, numerical modeling

© 2023 Author(s). All article content, except where otherwise noted, is licensed under a Creative Commons Attribution (CC BY) license (<http://creativecommons.org/licenses/by/4.0/>). <https://doi.org/10.2351/7.0001079>

I. INTRODUCTION

This paper provides in-depth numerical simulations of the keyhole mode technique in deep penetration laser beam welding of high-thickness components. The geometrical characteristics of the keyhole shape allow multiple reflections and corresponding absorption events, leading to enhanced total optical absorption.¹ Consequently, the net absorbed energy increases, enabling the joining of high-thickness components. Modern laser systems can deliver up to 100 kW of laser power, thus enabling single-pass laser beam welding of samples with a thickness of up to 50 mm.^{2,3} Hence, industrial applications can be found in shipbuilding,

aerospace, oil, and gas industries as well as in the manufacturing of thick-walled structures like pipelines and the production of vacuum vessels.

In the literature, many primary experimental studies attempted to improve the knowledge about the keyhole and the molten pool dynamics and their correlation with welding defects, e.g., porosity, spatter evolution, and hot cracking. Thereto, different monitoring and detection systems, utilizing techniques, such as acoustic measurements, high speed and infrared, as well as synchrotron x-ray imaging, were employed. These studies have provided deep insights into the laser beam welding process, e.g.,

06 September 2023 13:16:23

concerning the reconstruction of the three-dimensional weld pool surface,⁴ the real-time prediction of porosity defects,⁵ and the observation of geometrical weld characteristics of the keyhole and the melt pool as well as the absolute energy absorption amount during the welding process.^{6–8} While these experimental methods offer insights into the keyhole and molten pool dynamics, their application is often limited by their high cost, equipment requirements, and relatively low image resolution. Consequently, obtaining detailed information, such as transient flow patterns, velocity, and temperature distributions, remains challenging, making the solely experimental study of the laser beam welding process difficult.

In recent decades, computational technologies have advanced significantly, making numerical modeling a valuable research tool for estimating important process characteristics, such as thermal cycles, molten pool shape, and molten metal flow characteristics. Early numerical models focused solely on heat conduction, disregarding crucial physical aspects of the beam-matter interaction, such as multiple reflections, evaporation, and free surface deformation. Nonetheless, these somewhat simpler heat conduction or even analytical models can suffice, such as predicting the fusion zone, temperature distributions, and thermal cycles.⁹ However, the study of complex welding defects like pore formation and hot cracking necessitates a detailed description of the underlying physics, particularly the beam-matter interaction and thermofluid dynamics.

Hence, advanced computational fluid dynamics (CFD) numerical models that incorporate multiple reflections using a ray tracing technique were developed. These models precisely predict the energy distribution within the keyhole by calculating the location and direction of each subray's reflection. These models can be categorized into two-phase and three-phase models. Three-phase models account for solid, liquid, and gas phases,¹⁰ while two-phase models consider only the solid and liquid phases¹¹ sometimes including vapor-induced effects empirically.¹² An overview of available two-phase and three-phase models, along with a description of the considered physical phenomena, can be found in Ref. 13.

A review of existing laser beam welding numerical models reveals that a reliable model for studying keyhole and molten pool dynamics must accurately describe the temporal and spatial energy distribution on the keyhole wall, often achieved through ray tracing algorithms. Thereby, two-phase models that consider vapor-induced effects empirically strike a good balance between computational intensity and realistic results.

Hence, the main objective of the present study is to improve the numerical ray tracing approach, thus obtaining a more realistic prediction of the keyhole shape and molten pool dynamics for the laser beam welding process by process modeling. Four improvements were identified to improve the accuracy of the amount as well as the spatial and temporal distribution of the absorbed laser energy. These are as follows:

- Implementing a cosine condition in the search routine for the calculation of realistic reflection points.¹⁴
- Deriving a radius correction for the numerical mapping of the spatial Gaussian distribution of the initial laser beam.
- Mimicking the laser beam caustic by using different approximations for the converging and the diverging regions of the laser beam.

- Adopting a virtual mesh refinement approach to improve the general numerical accuracy of the ray tracing routine.^{15,16}

The study primarily focuses on the accuracy of the chosen ray tracing approach, which significantly impacts the energy distribution on the keyhole wall and, consequently, the keyhole and molten pool dynamics. To achieve this, a three-dimensional transient multiphysics numerical model was developed and compared with experimental measurements.

II. EXPERIMENTAL SETUP

Partial penetration welding experiments were done using unalloyed steel sheets S355J2+N of 12 mm thickness in the bead-on-plate mode. The sheet dimensions were $175 \times 100 \times 12$ mm³ being welded with a 16 kW disk laser Trumpf 16002 with a wavelength of 1030 nm. The focal diameter and the optical Rayleigh length were 500 μ m and 6.9 mm, respectively. The used welding parameters were as follows: laser power of 10 kW, focus position of -3 mm, and welding speed of 2.5 m/min with the laser torch being vertically aligned to the workpiece. 25 l/min Ar shielding gas was provided at a gas nozzle angle of 35°. Macro sections were cut from the middle region of the weld. For validation purposes, the metallographic cross sections have been prepared with a 2% nital etching.

III. NUMERICAL SETUP

A three-dimensional multiphysics thermofluid dynamics model with free surface tracking by the volume of fluid technique was developed. The simulations are based on previous work.^{17,18} Therefore, only major features of the model are repeated here. More emphasis was put on the improvements in the model, i.e., the implementation of the cosine condition to avoid wrong reflection points of the laser beam, the radius correction of the laser, the caustic mimicking by dividing the laser beam in converging and diverging parts, and the virtual mesh refinement approach.

The following assumptions were made to allow for a process simulation including strongly coupled, highly nonlinear interactions between the laser radiation, the vapor phase, the molten metal, and the solid material in reasonable computational times. The molten metal and the gas phase are assumed to be Newtonian and incompressible. The Reynolds number was assumed to be sufficiently small to allow a laminar fluid flow calculation. The Boussinesq approximation was used to model the impact of density variations on the flow.¹⁹ The computational domain was 32 mm in welding direction, 8 mm in width, and 14 mm in thickness direction (see Fig. 1). Hexahedral mesh cells with a minimum size of 0.2 mm were used leading to a total amount of approximately 370 000 control volumes.

The transport equations were solved with the commercial finite volume method software ANSYS Fluent. The spatial discretization of the momentum and energy conservation equations was realized by a second-order upwind scheme, and a first-order implicit formulation was applied for the discretization of transient terms. The pressure-velocity coupling was realized by the pressure-implicit with splitting of operators scheme. The computation was done on a high-performance computing cluster with 88 CPU cores at the Bundesanstalt für Materialforschung und -prüfung. The

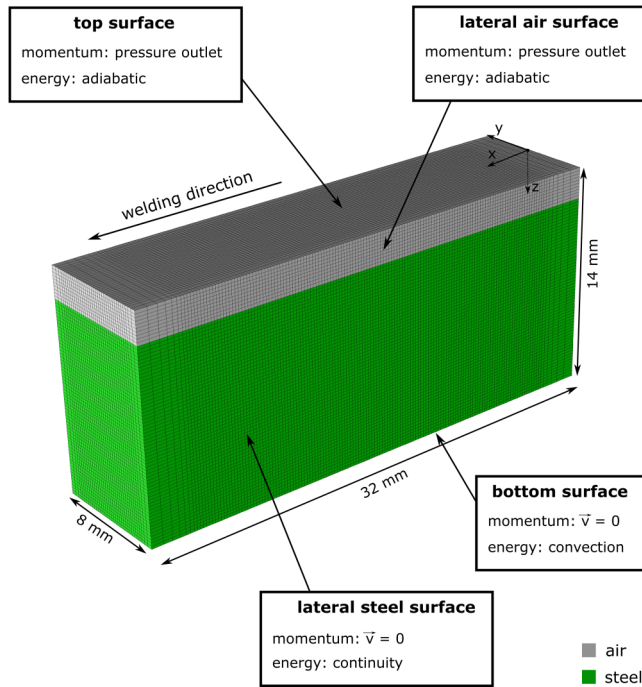


FIG. 1. Computational domain and boundary conditions.

average computing time was approximately 200 h for 0.6 s of real welding time.

Above the steel domain of 12 mm thickness, an air layer of 2 mm was defined to allow for interface tracking of the steel-air interface by the volume of fluid (VOF) method,²⁰

$$\frac{\partial \phi}{\partial t} + \nabla \cdot (\vec{v}\phi) = 0, \quad (1)$$

where t is the time, and the volume fraction of different phases (steel/gas) is denoted as ϕ .

The mass conservation and the Navier–Stokes equations describing the liquid flow in the model can be written as

$$\nabla \cdot \vec{v} = 0, \quad (2)$$

$$\rho \left(\frac{\partial \vec{v}}{\partial t} + \vec{v} \cdot \nabla \vec{v} \right) = -\nabla p + \mu \nabla^2 \vec{v} - \mu K \vec{v} + \vec{S}_m, \quad (3)$$

with the liquid metal flow velocity \vec{v} , the density ρ , pressure p , and the dynamic viscosity μ . K is the Carman–Kozeny equation coefficient for the enthalpy-porosity solidification model,^{21,22} and the volumetric force terms were summarized in \vec{S}_m including gravity, buoyancy,¹⁹ recoil pressure,²³ surface tension, and Marangoni stress.²⁴

The energy transport equation is as follows:

$$\rho \left[\frac{\partial h}{\partial t} + (\vec{v} \cdot \nabla) h \right] = \nabla \cdot (k \nabla T) + S_q, \quad (4)$$

with temperature T , thermal conductivity k , and enthalpy h . Additional energy source and sink terms, e.g., from the laser heat flux, convective heat losses, radiative losses, evaporation losses, and recondensation, were summarized in S_q . A multiple reflection ray tracing approach was utilized to calculate local laser absorption along the keyhole wall obeying Fresnel’s laws. More details of the numerical procedure, the material model used in this study, as well as detailed model validation can be found in the authors’ previous works.^{17,18}

The first improvement in the ray tracing model refers to a proper selection of the target reflection cell. In the standard ray tracing algorithm, a geometrical criterion is employed with a VOF-based free surface thereto instead of calculating the optically exact reflection point. A cell is identified as a potential target reflection cell when the shortest distance between the cell center and the reflected ray is smaller than a sphere surrounding that cell fulfilling the geometric condition $d \leq \sqrt{3}\Delta/2$ with cell size Δ ¹¹ (see Fig. 2). This approach identifies correct target cells when the angle between the incident ray and the outward surface normal is sufficiently small, see ray II in Fig. 2. If this angle comes close to 90° (see ray I in Fig. 2), the reflected ray can then be captured by the neighboring cell erroneously. This typically occurs in situations with a vertical laser beam and a steep keyhole wall. In consequence, the laser energy is transferred from one neighboring cell to the other causing an energy trapping in those areas of the keyhole. To avoid that, an

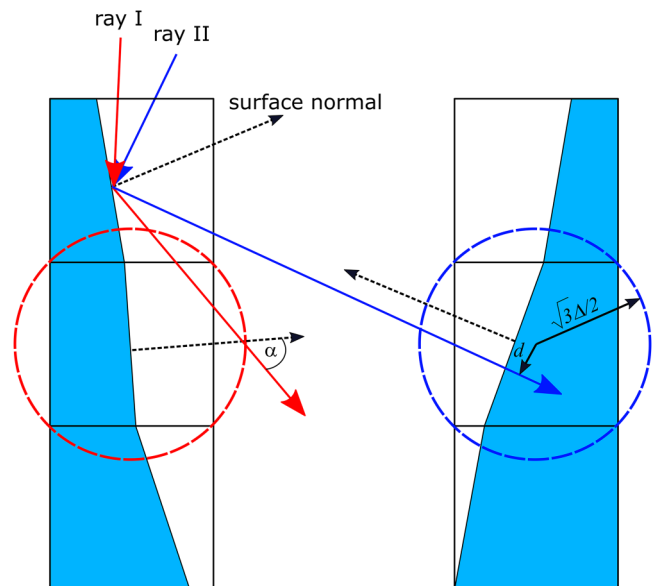


FIG. 2. Identification of reflection cells using a geometrical and a cosine condition.

06 September 2023 13:16:23

additional cosine criterion is applied for the potential reflection cells judging the angle between their incident ray and their outward normal vector. For optically wrong selected target cells (red circle in Fig. 2), this angle α is less than 90° . For correctly identified cells, this angle is always larger than 90° (blue circle in Fig. 2). This approach was validated in Ref. 14.

The second correction refers to an enhanced numerical treatment of the Gaussian distribution of the laser beam. Conventionally, the laser beam in numerical process models using the ray tracing technique is discretized in subrays with their relative position being located within the beam diameter. However, the beam diameter is defined by a decay of the laser intensity by a factor of $1/e^2$ at the focal position. Integrating the laser intensity over this so-defined laser beam area and normalizing this value with the nominal laser power yields

$$\frac{P(r, z)}{P_L} = 1 - \exp\left(-\frac{2r^2}{r_f^2(z)}\right), \quad (5)$$

with radius r and beam radius r_f . Hence, setting $r = r_f$ reveals that approximately only 86% of the initial laser beam energy is located there. Thus, around 14% of the initial laser energy is not available for the calculation of the subsequent distribution of the absorbed energy at the keyhole wall. For $r = 1.5 \cdot r_f$, it shows that the ratio of the discretized laser beam energy and the nominal laser energy is around 99%. According to that, the numerical model was improved

by considering a circle with a 150% radius of the beam radius for the discretization of the laser beam and the subsequent ray tracing routine, thus considering almost the whole amount of initial laser energy in the calculation.

Another improvement was realized by mimicking the beam caustic of the laser beam. The standard algorithm for its implementation included different laser intensities as well as incident angles for every subray. This approach allowed for a proper description of the area above the focal plane but failed in the area below [see Fig. 3(a)], as all the subrays are converging into a single point.²⁵ In a new approach, the laser beam was divided into a converging upper part and a diverging lower part with corresponding different incident angles of the subrays [see Fig. 3(b)], according to the optical laws and respecting the beam diameter in the focal plane. Thus, the beam caustic could be mimicked in the areas above and below the focal plane. Note that depending on the focal position and the depth of the specific weld and the Rayleigh length of the laser beam, only the lower, both, or only the upper part of the laser beam were needed for calculations [see Fig. 3(c)]. In cases, when the distance of the focal position to the weld bottom is much larger than the Rayleigh length, a further subdivision of the beam caustic can be required to obtain physically sound results [see Fig. 3(d)].

Thermo-fluid flow simulations of laser beam welding require a spatially precise calculation of laser beam absorption along the keyhole. As explained for the cosine condition, a geometric search criterion depending on the element size of the computational grid was used in the ray tracing algorithm to find potential target reflection cells. To keep the numerical procedure manageable in their computational costs, a minimum cell size of 0.2 mm in the order of the laser spot radius was used.²⁶ This choice may lead to inaccurate locations of the identified reflection points. An approach to improve the model accuracy to overcome this issue is a virtual mesh refinement of the identified potential reflection cells. This approach was described in detail in Refs. 15 and 16. The improvement in accuracy was achieved by the fact that the reduced virtual cell size can then be used in the criterion for the target reflection cell. As the virtual cells are only used in the search algorithm of the target reflection cells, the total computational effort of the fluid flow calculations is kept constant and brings no further iterations in the calculation of the governing equations. The principle of the virtual mesh refinement approach is shown in Fig. 4. In Ref. 17, it is shown that implementing a virtual mesh refinement procedure improved the calculated penetration depth to the value within the experimental scatter band, especially for higher welding speeds, where the results by the standard mesh procedure lead to a deviation of around 25%.

06 September 2023 13:16:23

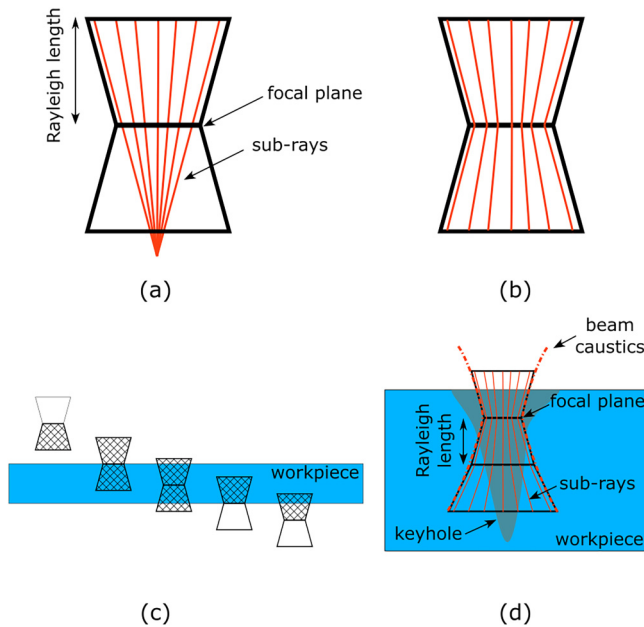


FIG. 3. (a) Subray orientation without considering the beam caustic, (b) subray orientation mimicking the beam caustic, (c) usage of different parts of the laser beam caustic in a CFD model, and (d) subdivision of the beam caustic.

IV. RESULTS AND DISCUSSION

The principal validation of the developed numerical model was already shown several times.^{17,18} In this work, the fusion line of the full model with all the presented model improvements applied is shown in Fig. 5. Here, the experimentally observed penetration depth of around 11.2 mm can be reproduced very well. The same holds for the weld width that is very close to the experimental result at different depths. The experimental weld shows almost no wine glass shape, which is a common issue to

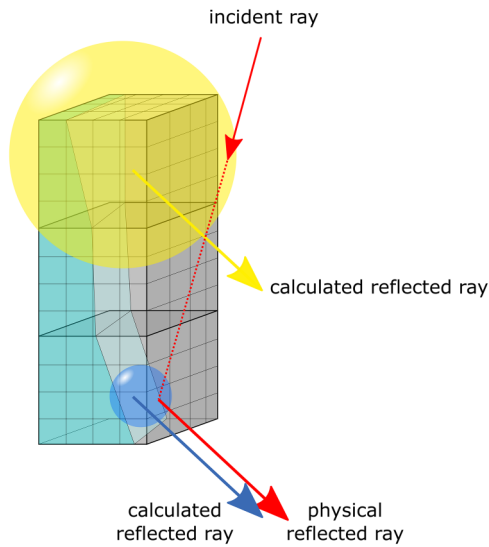


FIG. 4. Influence of the mesh size on the accuracy improvement in the search algorithm of the target reflection cell by the standard mesh size and the virtual mesh refinement approach.

be reproduced numerically with welding process models.¹² Figure 6 shows the comparison of the weld pool size and fluid flow in the longitudinal section for all different models investigated. Here, the full model with all improvements applied was

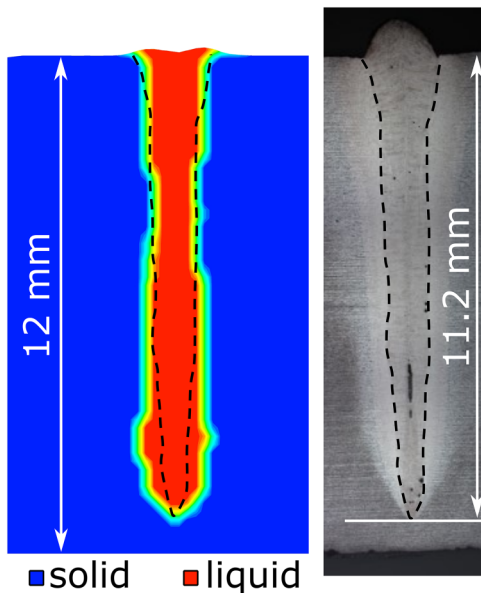


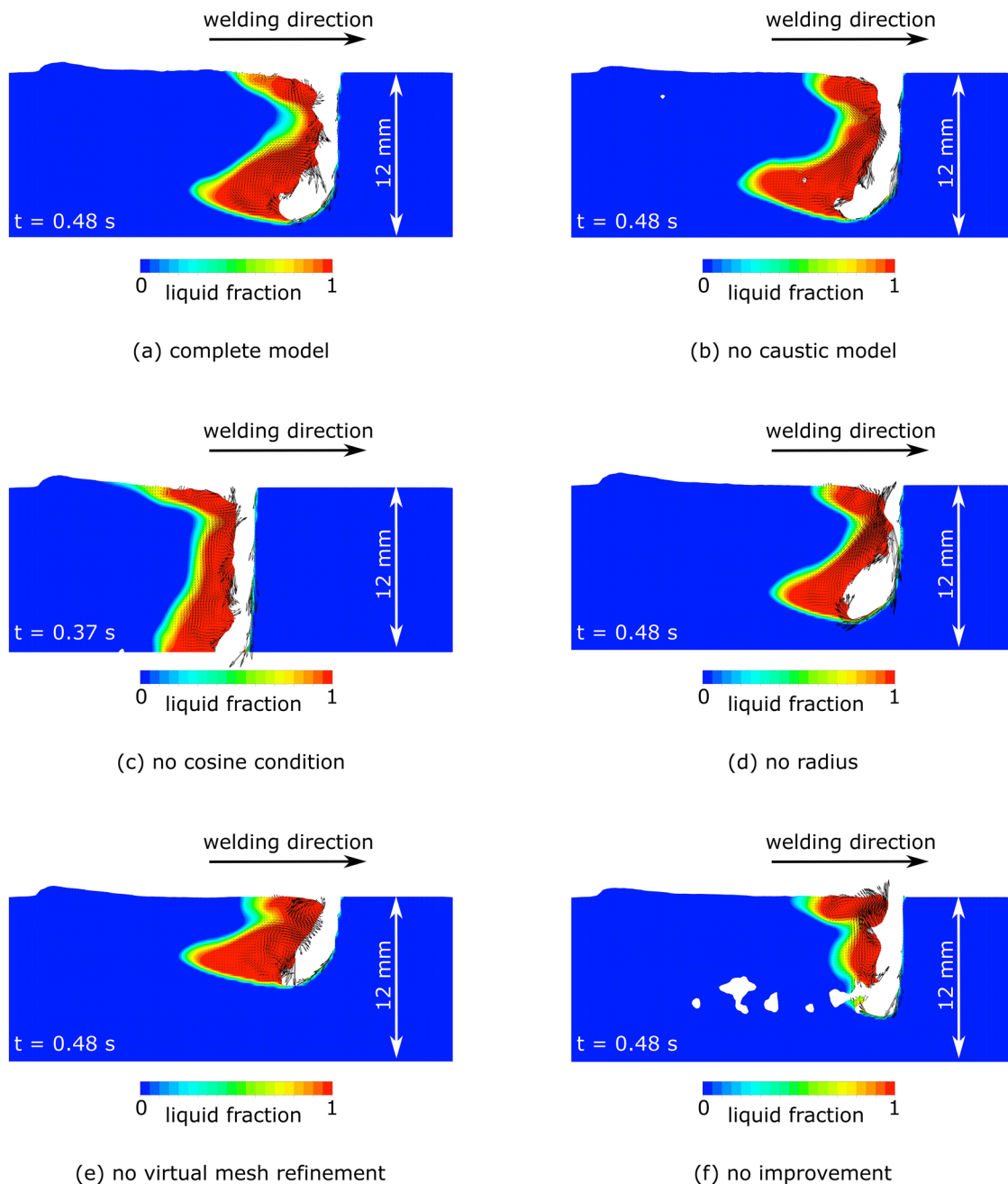
FIG. 5. Validation of the numerical model with experimental results.

chosen for comparison with the other models, with one improvement omitted in each case [Figs. 6(b)–6(e)] and without any improvements [Fig. 6(f)].

In Fig. 6(a), the shape of the weld pool is elongated at the upper surface, which is often seen in laser beam welding^{10,27} as a result of the Marangoni flow, enhanced flow in the opposite welding direction due to the recoil pressure, and the accelerated flow around the keyhole opening. In the bottom part, the weld pool shape is somewhat bulgy as often seen in other research^{12,18} associated with a pronounced recirculation zone caused by recoil pressure forces acting on the keyhole surface. Interestingly, the locations of the bulge area and the experimentally observed hot cracking coincide, most likely due to delayed local solidification and tensile stresses from solidification shrinkage in the surrounding at the same time.^{28,29} The model without mimicking the caustic geometry shows comparable results [Fig. 6(b)] with only minor differences in the upper part. This is expected in the region above the focal position [see Figs. 3(a) and 3(b)], and one can anticipate a more significant influence in the lower part of the weld pool for larger penetration depths, where the error for the uncorrected model becomes larger because of the unphysically higher laser energy density, cf. the bottom part of Figs. 6(a) and 6(b). Figure 6(c) shows the case without considering the cosine condition. As the keyhole wall has a steep angle, it is most likely that neighboring cells are erroneously identified as reflection target cells more often (cf. Fig. 2). In consequence, the laser energy is absorbed in a column of mesh cells at the keyhole front wall, thus drilling deeper into the material that leads to a narrower and deeper keyhole and weld pool. Note the shorter welding time shown compared to the other cases, as the simulation was canceled when reaching full penetration as the gas phase below the welding domain was not accounted for. Omitting the correction of the laser waist radius results in an obvious decrease in the absorbed laser energy. Consequently, the final penetration capacity is lower accordingly by about the same amount as the reduction in the absorbed energy, otherwise keeping the characteristics of the fluid flow in the weld pool. Not considering the virtual mesh refinement in the ray tracing algorithm results in a significant drop in the penetration depth of the weld pool [Fig. 6(e)], which is in line with previous research.¹⁷ Figure 6(f) shows the case when none of the proposed improvements is applied. Here, the penetration depth is smaller compared to the case in Fig. 6(a). The bulge region in the weld pool bottom is also much less pronounced as would be expected from Fig. 6(a) and experimental work.¹² Additionally, it seems that omitting all improvements in the model destabilizes the keyhole tip behavior as pore regions appear, see Fig. 6(f). Interestingly, the case without any improved elements still gives better penetration than the case without the virtual refinement of the ray tracing algorithm, cf. Figs. 6(e) and 6(f).

The averaged heat input for all simulation cases is shown in Fig. 7. Obviously, both cases without correcting the laser waist radius for the initial amount of the laser energy produce significantly less heat input with a process efficiency of approximately 80%. The other cases show only slight differences in the amount of absorbed laser energy with a total efficiency of around 90%–95%, which is slightly more than measured calorimetrically for AISI 304 stainless steel at 10 kW laser power.³⁰

06 September 2023 13:16:23



06 September 2023 13:16:23

FIG. 6. Comparison of the weld pool size and fluid flow in the longitudinal section.

Figure 8 shows the calculated keyhole depth for different simulation cases. A stable penetration depth can be confirmed for welding times above 100 ms, which is consistent with previous research.¹⁷ The caustic correction has only a minor influence on the keyhole depth, whereas the case without considering the virtual

refinement algorithm for the ray tracing shows a significant decrease in the keyhole depth. Interestingly, the heat input for this specific case and the numerically calculated melt volume is comparable to the case with all model improvements (approx. 38–42 mm³). One can conclude that not considering the virtual

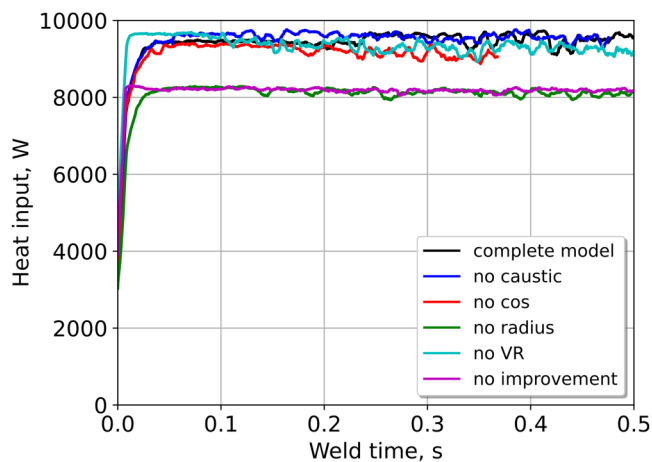


FIG. 7. Comparison of the averaged heat input in different models.

refinement causes a redistribution of the absorbed laser energy, which leads to bigger deviations from the experimental result and more molten material in the upper part of the weld bead due to a trapping effect of the laser rays there. This trapping effect was also shown in Ref. 17 for a welding speed of 2.5 m/min. The case without considering the cosine condition to exclude neighboring mesh cells to be regarded as target reflection cells leads to full penetration and accordingly the highest keyhole depth in Fig. 8. This case overestimates the drilling capacity of the laser beam and leads to a less developed weld pool flow in the upper region due to a lack of molten material.

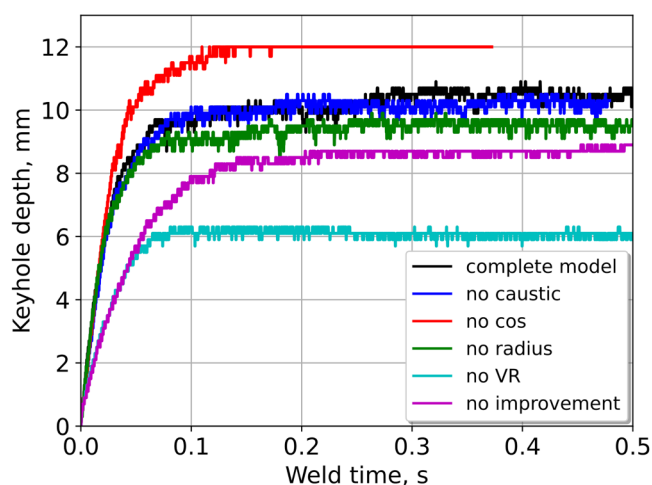


FIG. 8. Comparison of the calculated keyhole depth in different models.

V. CONCLUSIONS

In this study, four different improvements in the numerical modeling of the ray tracing algorithm during deep penetration laser beam welding are presented. These improvements comprise the search algorithm for target reflection cells by a cosine condition, the numerical treatment of the Gaussian distribution of the laser beam, mimicking the beam caustic by numerically dividing converging and diverging regions of the laser beam, and a virtual mesh refinement routine. The following conclusions can be drawn from the presented results:

- The developed three-dimensional transient multiphysics numerical model including all the improvements showed a very good agreement with experimental validation studies regarding the prediction of the final weld pool depth and the weld cross section.
- The caustic modeling improvement had no major influence in the weld top region but could have a potentially bigger influence in the bottom part for thicker welds typically having a much higher penetration depth compared to the Rayleigh length.
- The cosine condition was found to be essential for a correct prediction of laser reflection points and, thus, a realistic geometry of the melt pool.
- The radius correction did not change the weld pool geometry characteristics but had a distinct influence on the penetration depth.
- The virtual refinement algorithm in the ray tracing routine was found to be essential for a correct determination of the laser energy distribution along the keyhole and the final weld pool geometry and penetration depth.
- The standard algorithm without any improvements underestimated the penetration depth caused by trapping of the laser energy in the top region.

ACKNOWLEDGMENTS

This work was funded by the Deutsche Forschungsgemeinschaft (DFG, German Research Foundation) Project Nos. 411393804 (BA 5555/5-2), 416014189 (BA 5555/6-1), 466939224 (BA 5555/9-1), and 506270597 (ME 5634/1-1).

AUTHOR DECLARATIONS

Conflict of Interest

The authors have no conflicts to disclose.

Author Contributions

Marcel Bachmann: Conceptualization (equal); Data curation (equal); Formal analysis (equal); Funding acquisition (lead); Investigation (equal); Methodology (equal); Project administration (lead); Resources (lead); Supervision (equal); Validation (equal); Visualization (lead); Writing – original draft (lead); Writing – review & editing (lead). **Antoni Artinov:** Conceptualization (equal); Data curation (equal); Formal analysis (equal); Funding acquisition (equal); Investigation (equal); Methodology (equal); Software (equal); Validation (equal). **Xiangmeng Meng:**

Conceptualization (equal); Data curation (equal); Formal analysis (equal); Investigation (equal); Software (equal); Validation (equal); Visualization (equal); Writing – original draft (supporting); Writing – review & editing (supporting). **Stephen Nugraha Putra:** Data curation (equal); Formal analysis (equal); Software (equal). **Michael Rethmeier:** Funding acquisition (supporting); Project administration (supporting); Supervision (equal); Writing – original draft (supporting); Writing – review & editing (supporting).

REFERENCES

- ¹D. T. Swift-Hook and A. E. F. Gick, "Penetration welding with lasers," *Weld. J.* **52**, 492–499 (1973).
- ²X. Zhang, E. Ashida, S. Tarasawa, Y. Anma, M. Okada, S. Katayama, and M. Mizutani, "Welding of thick stainless steel plates up to 50 mm with high brightness lasers," *J. Laser Appl.* **23**, 022002 (2011).
- ³M. Bachmann, A. Gumenyuk, and M. Rethmeier, "Welding with high-power lasers: Trends and developments," *Phys. Proc.* **83**, 15–25 (2016).
- ⁴G. Saeed, M. Lou, and Y. M. Zhang, "Computation of 3D weld pool surface from the slope field and point tracking of laser beams," *Meas. Sci. Technol.* **15**, 389–403 (2004).
- ⁵M. Luo and Y. C. Shin, "Estimation of keyhole geometry and prediction of welding defects during laser welding based on a vision system and a radial basis function neural network," *Int. J. Adv. Manuf. Technol.* **81**, 263–276 (2015).
- ⁶C.-H. Kim and D.-C. Ahn, "Coaxial monitoring of keyhole during Yb:YAG laser welding," *Opt. Laser Technol.* **44**, 1874–1880 (2012).
- ⁷Y. Kawahito, Y. Uemura, Y. Doi, M. Mizutani, K. Nishimoto, H. Kawakami, M. Tanaka, H. Fujii, K. Nakata, and S. Katayama, "Elucidation of the effect of welding speed on melt flows in high-brightness and high-power laser welding of stainless steel on basis of three-dimensional X-ray transmission *in situ* observation," *Weld. Int.* **31**, 206–213 (2017).
- ⁸B. J. Simonds, J. Tanner, A. Artusio-Glimpse, P. A. Williams, N. Parab, C. Zhao, and T. Sun, "The causal relationship between melt pool geometry and energy absorption measured in real time during laser-based manufacturing," *Appl. Mater. Today* **23**, 101049 (2021).
- ⁹V. A. Karkhin, P. N. Khomich, and V. G. Michailov, "Models for volume heat sources and functional-analytical technique for calculating the temperature fields in butt welding," in *Mathematical Modelling of Weld Phenomena* (Verlag der Technischen Universitaet Graz, Graz, 2007), pp. 819–834.
- ¹⁰A. Otto, H. Koch, K.-H. Leitz, and M. Schmidt, "Numerical simulations—A versatile approach for better understanding dynamics in laser material processing," *Phys. Proc.* **12**, 11–20 (2011).
- ¹¹J.-H. Cho and S.-J. Na, "Implementation of real-time multiple reflection and fresnel absorption of laser beam in keyhole," *J. Phys. D: Appl. Phys.* **39**, 5372–5378 (2006).
- ¹²S. Muhammad, S.-W. Han, S.-J. Na, A. Gumenyuk, and M. Rethmeier, "Study on the role of recondensation flux in high power laser welding by computational fluid dynamics simulations," *J. Laser Appl.* **30**, 012013 (2018).
- ¹³J. Svenungsson, I. Choquet, and A. F. H. Kaplan, "Laser welding process—A review of keyhole welding modelling," *Phys. Proc.* **78**, 182–191 (2015).
- ¹⁴X. Meng, M. Bachmann, A. Artinov, and M. Rethmeier, "A study of the magnetohydrodynamic effect on keyhole dynamics and defect mitigation in laser beam welding," *J. Mater. Process. Technol.* **307**, 117636 (2022).
- ¹⁵M. Bachmann, X. Meng, A. Artinov, and M. Rethmeier, "Elucidation of the bulging effect by an improved ray-tracing algorithm in deep penetration wire feed laser beam welding and its influence on the mixing behavior," *Adv. Eng. Mater.* 2101299 (2022).
- ¹⁶X. Meng, S. N. Putra, M. Bachmann, A. Artinov, and M. Rethmeier, "Influence of the free surface reconstruction on the spatial laser energy distribution in high power laser beam welding modeling," *J. Laser Appl.* **34**, 042023 (2022).
- ¹⁷A. Artinov, X. Meng, M. Bachmann, and M. Rethmeier, "Numerical analysis of the high power laser beam welding of thick sheets at high process speeds," *Metals* **11**, 1319 (2021).
- ¹⁸A. Artinov, X. Meng, M. Bachmann, and M. Rethmeier, "Study on the transition behavior of the bulging effect during deep penetration laser beam welding," *Int. J. Heat Mass Transfer* **184**, 122171 (2022).
- ¹⁹T. E. Faber, *Fluid Dynamics for Physicists* (Cambridge University Press, Cambridge, 1995).
- ²⁰C. W. Hirt and B. D. Nichols, "Volume of fluid (VOF) method for the dynamics of free boundaries," *J. Comput. Phys.* **39**, 201–225 (1981).
- ²¹C. Prakash, M. Samonds, and A. K. Singhal, "A fixed grid numerical methodology for phase change problems involving a moving heat source," *Int. J. Heat Mass Transfer* **30**, 2690–2694 (1987).
- ²²A. D. Brent, V. R. Voller, and K. J. Reid, "Enthalpy-porosity technique for modeling convection-diffusion phase change: Application to the melting of a pure metal," *Numer. Heat Transfer* **13**, 297–318 (1988).
- ²³V. Semak and A. Matsunawa, "The role of recoil pressure in energy balance during laser materials processing," *J. Phys. D: Appl. Phys.* **30**, 2541–2552 (1997).
- ²⁴K. C. Mills, B. J. Keene, R. F. Brooks, and A. Shirali, "Marangoni effects in welding," *Philos. Trans. R. Soc. London Ser. A* **356**, 911–925 (1998).
- ²⁵W.-I. Cho, S.-J. Na, C. Thomy, and F. Vollertsen, "Numerical simulation of molten pool dynamics in high power disk laser welding," *J. Mater. Process. Technol.* **122**, 262–275 (2012).
- ²⁶W.-I. Cho and S.-J. Na, "Impact of wavelengths of CO₂, disk, and green lasers on fusion zone shape in laser welding of steel," *J. Weld. Join.* **38**, 235–240 (2020).
- ²⁷N. Bakir, Ö. Üstündag, A. Gumenyuk, and M. Rethmeier, "Influence of the weld pool geometry on solidification cracking in partial penetration high power laser beam welding," *Proc. CIRP* **111**, 397–400 (2022).
- ²⁸C. Cross, "On the origin of weld solidification cracking," in *Hot Cracking Phenomena in Welds* (Springer, Berlin, Heidelberg, 2005), pp. 3–18.
- ²⁹A. Artinov, M. Bachmann, X. Meng, V. Karkhin, and M. Rethmeier, "On the relationship between the bulge effect and the hot cracking formation during deep penetration laser beam welding," *Proc. CIRP* **94**, 5–10 (2020).
- ³⁰Y. Kawahito, N. Matsumoto, Y. Abe, and S. Katayama, "Relationship of laser absorption to keyhole behavior in high power fiber laser welding of stainless steel and aluminum alloy," *J. Mater. Process. Technol.* **211**, 1563–1568 (2011).